J. Fluid Mech. (1983), *vol.* 130, *pp.* 299–314
Printed in Great Britain

Longitudinal dispersion coefficients for varying channels

By RONALD SMITH

Department of Applied Mathematics and Theoretical Physics, University of Cambridge, Silver Street, Cambridge CB3 9EW

(Received 5 April 1982)

A general expression is obtained for the longitudinal dispersion coefficient for a passive contaminant in a varying channel. This expression reveals the upstream memory character of the dispersion coefficient. Simple examples are used to illustrate the effects of: a sudden change in breadth, centrifugally driven secondary flows, and changes in the depth profile.

1. Introduction

Although most flows in nature vary along their length, most theoretical work on longitudinal contaminant dispersion has concerned longitudinally uniform channels. Fischer (1969) pointed out that it is justifiable to use such a uniform model only if the lengthscale for mixing across the channel is less than the lengthscale for channel variations. In practice, the diffusion lengthscale in natural streams is of the order of 100 channel breadths and can greatly exceed the bend-length.

Fischer (1969) showed how the longitudinal dispersion coefficient could be computed for periodic bends. The effect of longitudinal non-uniformity can be quite marked. In a numerical model of a stretch of the Missouri River, Fischer found that the longitudinal dispersion coefficient was nearly a factor of 10 smaller than would have been the case of a longitudinally uniform channel. The qualitative explanation is that the effective current (averaged over a diffusion length-scale) can be much less strongly sheared than the current at each individual transect, and the shear-dispersion process is correspondingly weakened.

The objective of the present work is to provide an analytic counterpart to Fischer's (1969) computational scheme. A formula is obtained for the (positive) bend-averaged longitudinal dispersion coefficient. To utilize this formula it is mathematically convenient, and physically natural, to use the concept of a local shear-dispersion coefficient. This local value has an upstream memory over a diffusion lengthscale, and can be negative (as has been observed experimentally by Fukuoka & Sayre 1973). Simple examples are used to illustrate the behaviour both of the local and of the bend-averaged dispersion coefficients.

2. Advection–diffusion equation

For a channel that is much wider than it is deep, the timescale for cross-sectional mixing is much greater than that for vertical mixing. Thus, in a study of the even slower process of longitudinal dispersion, the contaminant can be regarded as being vertically well-mixed. Also, in the absence of abrupt features (such as stone jetties), the transverse lengthscales of the turbulence are much less than the channel width, so it is justifiable to use an eddy-diffusivity model for the transverse mixing.

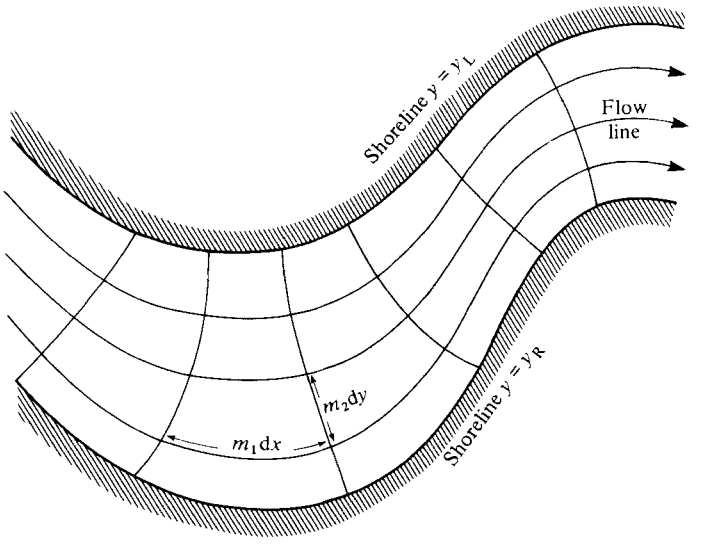

FIGURE 1. Orthogonal curvilinear coordinate system for a meandering stream.

Hence, as the starting-point of our mathematical analysis, we shall assume that the depth-averaged concentration c satisfies the advection–diffusion equation

$$h\partial_t c + h\mathbf{u}\cdot\nabla c - \nabla\cdot(h\boldsymbol{\kappa}\cdot\nabla c) = 0, \tag{2.1a}$$

with

$$h\mathbf{n}\cdot\mathbf{u} = h\mathbf{n}\cdot\boldsymbol{\kappa}\cdot\nabla c = 0, \tag{2.1b}$$

on the banks and

$$\nabla\cdot(h\mathbf{u}) = 0. \tag{2.1c}$$

Here h is the water depth, $\mathbf{u}$ the depth-averaged flow velocity, $\boldsymbol{\kappa}$ the horizontal dispersion tensor (i.e. turbulence plus any contribution from the vertical shear dispersion associated with secondary currents), ∇ the horizontal gradient operator, and $\mathbf{n}$ the outward normal at the river banks.

Relative to the horizontal length and advection velocity scales, the dispersion tensor $\boldsymbol{\kappa}$ is numerically very small (i.e. $\boldsymbol{\kappa}$ scales as the product of the water depth and the friction velocity). Thus advection is dominant along the flow, diffusion only being important across the flow.

A technical difficulty for the mathematical analysis of any aspect of contaminant dispersion in natural waterways is that the flow lines, and hence the contaminant, can wander back and forth across the principal channel direction. To deal with this, Fischer (1969) formulated his numerical method in terms of stream tubes. For studies of contaminant dispersion across rivers, the use of flow-following coordinates has been developed further by Yotsukura & Cobb (1972) and Yotsukura & Sayre (1976).

With such a coordinate system (x, y) aligned along and across the flow (see figure 1), it is straightforward to identify the cross-stream component κ_{22} of the dispersion and to retain just the important features of the advection–diffusion equation (2.1):

$$m_1 m_2 h\partial_t c + m_2 hu\,\partial_x c - \partial_y\left(\frac{m_1}{m_2} h\kappa_{22}\partial_y c\right) = 0, \tag{2.2a}$$

with

$$hu = h\kappa_{22}\partial_y c = 0 \quad (y = y_R, y_L), \tag{2.2b}$$

$$\partial_x(m_2 hu) = 0. \tag{2.2c}$$

Here $m_1(x, y)$, $m_2(x, y)$ are metric coefficients and y_R, y_L denote the right and left channel sides (facing downstream).

The unfamiliarity of calculations involving the metric coefficients is minimized by our making the requirement that the longitudinal distance increment m_1 is adjusted so that

$$A = \int_{y_R}^{y_L} m_2 h \, dy = \int_{y_R}^{y_L} m_1 m_2 h \, dy. \tag{2.3}$$

Thus the incremental volume between adjacent x-contours is the same as the conventional cross-sectional area A. Also, it is convenient to include the m_1 factor in the definition of cross-sectional average values:

$$\bar{f} = \frac{1}{A} \int_{y_R}^{y_L} f m_1 m_2 h \, dy. \tag{2.4}$$

For the longitudinal velocity the rate of crossing of x-contours is given by

$$u_1 = u/m_1. \tag{2.5}$$

The cross-sectional average value $\bar{u}_1$ is the same as the conventional definition of the bulk velocity, and conservation of volume flow along the channel can be expressed as

$$A\bar{u}_1 = \text{constant}. \tag{2.6}$$

3. Two lengthscales

As the cross-sectionally averaged velocity $\bar{u}_1(x)$ increases and decreases (i.e. as the channel narows and widens), the contaminant cloud will appear to undergo concertina-like deformations. To deal with this we introduce a moving coordinate system

$$\xi = \epsilon U \left(\int_0^x \frac{dx'}{\bar{u}_1(x')} - t \right), \tag{3.1a}$$

$$\tau = \epsilon^2 t, \tag{3.1b}$$

where U is any convenient reference velocity. Thus, in the (ξ, τ)-coordinates, any evolution of the bulk concentration is associated with dispersion and not merely the non-uniform advection. The presence of the parameter ϵ serves to indicate that the longitudinal lengthscale ξ of the contaminant cloud is to be thought of as being much longer than the lengthscale x for mixing across the channel, with a correspondingly slow timescale τ for the longitudinal dispersion.

The channel topography does not move along with the (ξ, τ)-coordinate system. Thus the comparatively small and rapidly changing variations in concentration across the flow (associated with the velocity and depth profiles) are best described in the stationary (x, y)-coordinates. The method of multiple scales (Nayfeh 1973, chap. 6) was developed to deal with precisely this type of situation. We regard c as a function of both ξ and x, and in the equation for $c(x, y, \xi, \tau)$ we retain both ξ and x-derivatives:

$$m_1 m_2 u_1 \partial_x c - \partial_y \left(\frac{m_1}{m_2} h \kappa_{22} \partial_y c \right) + \epsilon \frac{U}{\bar{u}_1} m_1 m_2 h (u_1 - \bar{u}_1) \partial_\xi c + \epsilon^2 m_1 m_2 h \partial_\tau c = 0. \tag{3.2}$$

In the solution procedure the decomposition between ξ- and x-behaviour is organized so that on the short x-scale there is no systematic growth.

4. The shape of the function G

Following Taylor (1953) or Fischer (1967, 1969), we assume that the timescale $\tau = \epsilon^2 t$ upon which we are studying the dispersion process is sufficiently long that the contaminant is nearly uniformly distributed across the flow, and does not vary much on the scale of a single bend:

$$c = c_0(\xi, \tau) + \epsilon c_1(x, y, \xi, \tau) + \epsilon^2 c_2(x, y, \xi, \tau) + \ldots. \tag{4.1}$$

Also, without loss of generality, we can require that the correction terms $c_1, c_2, \ldots$ give no net contribution to the concentration when integrated over the entire flow.

From equation (3.2) it follows that to a first approximation c_1 satisfies the equation

$$m_1 m_2 h u_1 \partial_x c_1 - \partial_y\left(\frac{m_1}{m_2} h \kappa_{22} \partial_y c_1\right) = \frac{U}{\bar{u}_1} m_1 m_2 h(\bar{u}_1 - u_1)\,\partial_\xi c_0, \tag{4.2a}$$

with

$$h\kappa_{22}\partial_y c_1 = 0 \quad (y = y_R, y_L), \tag{4.2b}$$

$$\langle A\bar{c}_1 \rangle = 0. \tag{4.2c}$$

Here the angle brackets $\langle \ldots \rangle$ denote bend averaging:

$$\langle f \rangle = \frac{1}{2L}\int_{x-L}^{x+L} f \,\mathrm{d}x. \tag{4.3}$$

For periodic bends $2L$ is the bend length, while for non-periodic bends L has to be sufficiently large for the averages to become effectively independent of L.

To solve (4.2) we introduce the auxiliary function $G(x, y)$:

$$m_1 m_2 h u_1 \partial_x G - \partial_y\left(\frac{m_1}{m_2} h \kappa_{22} \partial_y G\right) = m_1 m_2 h(\bar{u}_1 - u_1)/\bar{u}_1, \tag{4.4a}$$

with

$$h\kappa_{22}\partial_y G = 0 \quad (y = y_R, y_L), \tag{4.4b}$$

$$\overline{u_1 G} = 0. \tag{4.4c}$$

We remark that by construction $G(x, y)$ is independent of the choice of the reference velocity U. The particular normalization (4.4c) has been chosen because on integrating (4.4a) across the flow we find that

$$\frac{\partial}{\partial x}\int_{y_R}^{y_L} m_1 m_2 h u_1 G \,\mathrm{d}y = 0. \tag{4.5}$$

On the right-hand side of (4.2a) the $\partial_\xi c_0$ factor can be regarded as remaining constant on the x-lengthscale. Thus, we can represent c_1 as

$$c_1 = U\left(G - \frac{\langle \bar{G} A \rangle}{\langle A \rangle}\right)\partial_\xi c_0, \tag{4.6}$$

where the constant (bend-averaged) term has been included to ensure that c_1 gives no net contribution to the concentration. From (4.6) we see that $G(x, y)$ gives the shape of the concentration profile across the flow.

5. Longitudinal-dispersion equation

The vital contribution of Taylor (1953) to the theory of contaminant dispersion was to recognize that, without the c_1 correction term in the presentation (4.1), there is no shear dispersion, only the comparatively weak mechanism of longitudinal

diffusion. In (2.2*a*) we have already neglected longitudinal diffusion. Thus the role of c_1 is highlighted when we cross-sectionally and bend-average (3.2) to derive an evolution equation for c_0:

$$\langle A\rangle \partial_\tau c_0 + \left\langle \frac{U}{\bar{u}_1} \overline{A(u_1-\bar{u}_1)\,\partial_\xi c_1} \right\rangle = O(\epsilon), \tag{5.1}$$

i.e. in the moving axes $c_0(\xi,\tau)$ would remain fixed (independent of τ) if c_1 were absent. Mathematically (5.1) can be recognized as a non-secularity condition which ensures that the solution for c_2 has no systematic growth with respect to x.

Substituting the result (4.6) into (5.1), we arrive at the longitudinal dispersion equation

$$\langle A\rangle \partial_\tau c_0 - U^2 \langle A\bar{G}\rangle \partial_\xi^2 c_0 = 0. \tag{5.2}$$

If we multiply (4.4*a*) by $G(x,y)$ and integrate across the flow, then we can derive the identity

$$A\bar{G} = \int_{y_R}^{y_L} \frac{m_1}{m_2} \kappa_{22} (\partial_y G)^2 \,\mathrm{d}y + \frac{1}{2}\frac{\partial}{\partial x}(\overline{A u_1 G^2}). \tag{5.3}$$

On the right-hand side the first term is strictly positive, and the second term has zero average with respect to x. Thus, as we should expect, the diffusion coefficient in (5.2) is positive.

For reasons which become apparent in the next section we choose to re-write equation (5.2)

$$\partial_\tau c_0 - \left(\frac{\langle A\rangle U}{A\bar{u}_1}\right)^2 D\,\partial_\xi^2 c_0 = 0, \tag{5.4}$$

where the bend-averaged shear-dispersion coefficient D is given by

$$D = \frac{\langle A^3 \bar{u}_1^2 \bar{G}\rangle}{\langle A\rangle^3}. \tag{5.5}$$

We remark that for periodic bends a convenient choice for the reference velocity would be to make

$$\langle A\rangle U = A\bar{u}_1. \tag{5.6}$$

6. Local shear-dispersion coefficient

If we revert to the use of (x,t)-coordinates then the above results (4.1), (4.6) take the form

$$c = c_0 + \bar{u}_1 \left(G - \frac{\langle A\bar{G}\rangle}{\langle A\rangle}\right) \partial_x c_0 + \ldots. \tag{6.1}$$

Replacing c_0 by the local cross-sectionally averaged concentration $\bar{c}$ we have instead (Fischer 1967, equation (11))

$$c = \bar{c} + \bar{u}_1 (G - \bar{G})\,\partial_x \bar{c} + \ldots. \tag{6.2}$$

Substituting this into (2.2*a*) and integrating across the flow, we arrive at the longitudinal dispersion equation

$$A(\partial_t \bar{c} + \bar{u}_1 \partial_x \bar{c}) - \partial_x (A D_{\mathrm{loc}} \partial_x \bar{c}) = 0, \tag{6.3}$$

where the local shear-dispersion coefficient D_{loc} is given by

$$D_{\mathrm{loc}} = -\overline{(u_1-\bar{u}_1)(G-\bar{G})}\,\bar{u}_1 = \bar{u}_1^2 \bar{G} \tag{6.4}$$

(Fischer 1976, equation (17)).

Starting from (6.4) and transferring to moving axes, we can rederive (5.4) with

$$D = \left\langle \left(\frac{A}{\langle A\rangle}\right)^3 D_{\mathrm{loc}} \right\rangle. \tag{6.5}$$

The concertina effect makes the contaminant cloud change its length, with the local value of $\partial_x^2 \bar{c}$ varying as $(A/\langle A\rangle)^2$ (Smith 1977, equation (3c)). This preferential weighting in favour of the wider slower-moving regions is further compounded by an extra factor $A/\langle A\rangle$ to allow for the extra time spent by the contaminant cloud in these regions.

By virtue of the relationship (6.5) the local dispersion coefficient D_{loc} provides us with more information and insight to the dispersion process than does the averaged quantity D. Unfortunately, the same cannot be said of the local equation (6.3). As can be seen from (5.3), if $\overline{u_1 G^2}$ varies rapidly along the flow, then there can be short sections of the channel in which D_{loc} is negative. Such local reductions in size of the contaminant cloud have been observed in laboratory experiments by Fukuoka & Sayre (1973). Alas, diffusion equations such as (6.3) become ill-conditioned when the diffusion coefficient is negative. To suppress the spurious instabilities it would be necessary to extend (6.2), (6.3) to include higher-order corrections. Of course, the bend-averaged equation (5.4) is free of such difficulties.

7. Eigenfunction expansions

An intrinsic feature for varying channels is the memory character of the dispersion process (over a diffusion lengthscale). To accommodate this feature in the selection of discharge sites, Smith (1982) introduced generalized eigenmodes for diffusion across the flow. Here it is shown how these functions can be used to solve (4.4a–c) for the shape factor G and to derive a general expression for the longitudinal-dispersion coefficient.

We define eigenmodes going with and against the flow:

$$\partial_y\left(\frac{m_1}{m_2} h\kappa_{22}\partial_y \phi_n^{(+)}\right) + \mu_n m_1 m_2 h u_1 \phi_n^{(+)} = m_1 m_2 h u_1 \partial_x \phi_n^{(+)}, \tag{7.1a}$$

$$\partial_y\left(\frac{m_1}{m_2} h\kappa_{22}\partial_y \phi_n^{(-)}\right) + \mu_n m_1 m_2 h u_1 \phi_n^{(-)} = -m_1 m_2 h u_1 \partial_x \phi_n^{(-)}, \tag{7.1b}$$

with

$$h\kappa_{22}\partial_y \phi_n^{(+)} = h\kappa_{22}\partial_y \phi_n^{(-)} = 0 \quad (y = y_{\mathrm{R}}, y_{\mathrm{L}}), \tag{7.1c}$$

$$\overline{u_1 \phi_n^{(+)}\phi_n^{(-)}} = \bar{u}_1, \quad \overline{u_1 \phi_n^{(+)}\phi_j^{(-)}} = 0 \quad (n \neq j), \tag{7.1d}$$

$$\overline{u_1 \phi_n^{(+)}\partial_x \phi_n^{(-)}} = \overline{u_1 \phi_n^{(-)}\partial_x \phi_n^{(+)}} = 0 \tag{7.1e}$$

(Smith 1982). These adjoint functions $\phi_n^{(+)}(x,y)$, $\phi_n^{(-)}(x,y)$ with their shared eigenvalue $\mu_n(x)$, permit us to deal with varying flow geometries almost as if there was no x-dependence. The zero mode is $\phi_0^{(+)} = \phi_0^{(-)} = 1$, corresponding to uniform concentration across the flow.

Since the equation (4.4a) for $G(x,y)$ involves an x-derivative in the flow direction, it is natural for us to seek a solution in terms of the + modes:

$$G(x,y) = \sum_{n=1}^{\infty} G_n(x)\,\phi_n^{(+)}(x,y). \tag{7.2}$$

To have a compatible representation for the right-hand-side term in (4.4*a*), we put

$$m_1 m_2 h(\bar{u}_1 - u_1) = m_1 m_2 h u_1 \sum_{n=1}^{\infty} \overline{\phi_n^{(-)}} \phi_n^{(+)}(x, y), \tag{7.3}$$

where, by virtue of the orthogonality of $\phi_n^{(-)}$ and $\phi_0^{(+)} = 1$, we have

$$\overline{(\bar{u}_1 - u)\,\phi_n^{(-)}} = \bar{u}_1 \overline{\phi_n^{(-)}}. \tag{7.4}$$

The $\phi_n^{(+)}$ component of (4.4*a*) yields a first-order ordinary differential equation for G_n:

$$\frac{\mathrm{d}G_n}{\mathrm{d}x} + \mu_n(x)\, G_n = \frac{\overline{\phi_n^{(-)}}(x)}{\bar{u}_1(x)}. \tag{7.5}$$

The resulting composite solution for $G(x, y)$ is

$$G = \sum_{n=1}^{\infty} \phi_n^{(+)} \int_{-\infty}^{x} \frac{\overline{\phi_n^{(-)}}(x')}{\bar{u}_1(x')} \exp\left(-\int_{x'}^{x} \mu_n(x'')\, \mathrm{d}x'' \right) \mathrm{d}x'. \tag{7.6}$$

By hypothesis, the lengthscale over which the contaminant cloud has been evolving is well in excess of the diffusion lengthscale. That is why the integrals formally extend arbitrarily far upstream.

The corresponding formula for the local shear-dispersion coefficient (6.4) is

$$D_{\mathrm{loc}} = [\bar{u}_1(x)]^2 \sum_{n=1}^{\infty} \overline{\phi_n^{(+)}}(x) \int_{-\infty}^{x} \frac{\overline{\phi_n^{(-)}}(x')}{\bar{u}_1(x')} \exp\left(-\int_{x'}^{x} \mu_n(x'')\, \mathrm{d}x'' \right) \mathrm{d}x'. \tag{7.7}$$

The upstream-memory character of this expression is in accord with Fukuoka & Sayre's (1973) experimental observation that the local dispersion coefficient lags behind the velocity shear. For uniform flows $\overline{\phi_n^{(+)}} = \overline{\phi_n^{(-)}}$ and the dispersion coefficient is strictly positive. Any negativeness of D_{loc} is necessarily associated with opposed signs of the $\overline{\phi_n^{(+)}}$, $\overline{\phi_n^{(-)}}$ factors, i.e. with pronounced changes in the flow.

8. Long and short bends

If the lengthscale $1/\mu_1$ for cross-sectional mixing is much less than the distance between the bends, then the $u_1 \partial_x$ terms are negligible in the eigenfunction equations (7.1*a*, *b*). Thus we have $\phi_n^{(+)} = \phi_n^{(-)}$, and the local dispersion coefficient (7.7) can be approximated as

$$D_{\mathrm{loc}} = \bar{u}_1(x) \sum_{n=1}^{\infty} \frac{\overline{(\phi_n^{(+)}(x))^2}}{\mu_n(x)}. \tag{8.1}$$

Hence the bend-averaged dispersion coefficient (6.5) is dominated by regions of large A^2/μ_n, i.e. regions of great width or of weak mixing across the flow where the shear-dispersion mechanism is locally very efficient.

In the opposite limit of short bends, it is the $u_1 \partial_x$ terms that dominate in the equations (7.1*a*, *b*) for the first few eigenfunctions. Thus, to a first approximation, $\phi_n^{(+)}$ is independent of x:

$$\phi_n^{(+)} \sim \langle \phi_n^{(+)} \rangle. \tag{8.2}$$

Denoting the leading correction term as $\psi_n^{(+)}$, we have

$$m_1 m_2 h u_1 \partial_x \psi_n^{(+)} = \partial_y \left(\frac{m_1}{m_2} h \kappa_{22} \partial_y \langle \phi_n^{(+)} \rangle \right) + \mu_n m_1 m_2 h u_1 \langle \phi_n^{(+)} \rangle. \tag{8.3}$$

Averaging this equation around the bends, we find that

$$\partial_y\left(\left\langle\frac{m_1}{m_2}h\kappa_{22}\right\rangle\partial_y\langle\phi_n^{(+)}\rangle\right)+\langle\mu_n m_1 m_2 hu\rangle\langle\phi_n^{(+)}\rangle=0, \tag{8.4}$$

with precisely the same equation for $\langle\phi_n^{(-)}\rangle$. Also, substituting for $\partial_x\phi_n^{(+)}=\partial_x\psi_n^{(+)}$ into (7.1*e*), we can evaluate the local eigenvalue

$$\mu_n(x)=\frac{1}{A\bar{u}_1}\int_{y_R}^{y_L}\frac{m_1}{m_2}h\kappa_{22}(\partial_y\langle\phi_n^{(+)}\rangle)^2\,\mathrm{d}y. \tag{8.5}$$

Since the memory distance $1/\mu_n$ extends over several bends, we find that the longitudinal-dispersion coefficient (7.7) varies as the square of the local bulk velocity:

$$D_{\mathrm{loc}}=\bar{u}_1(x)^2\left(\sum_{n=1}^{\infty}\frac{\overline{\langle\phi_n^{(+)}\rangle^2}}{\langle\mu_n\rangle}\right)\left\langle\frac{1}{\bar{u}_1}\right\rangle, \tag{8.6a}$$

$$D=\frac{A\bar{u}}{\langle A\rangle}\sum_{n=1}^{\infty}\frac{\overline{\langle\phi_n^{(+)}\rangle^2}}{\langle\mu_n\rangle}. \tag{8.6b}$$

In contrast with the long-bend result (8.1), the expression (8.6*a*) for D_{loc} involves the reciprocal of the averaged eigenvalue $1/\langle\mu_n\rangle$, and not the reciprocal of the local value $1/\mu_n$. Thus the dominant contributions arise where the cross-stream mixing is strong, i.e. regions of narrow width where the dispersion mechanism is inefficient. Hence, in accord with Fischer's (1969) numerical computations for a stretch of the Missouri River, short bends are associated with greatly reduced longitudinal-dispersion coefficients as compared with long bends.

9. Self-similar depth profiles

For straight channels the turbulent diffusivities for mass and for momentum scales as the product of the water depth h and the friction velocity u_* (Elder 1959). If we model u_* as being proportional to the local depth-averaged advection velocity u and we take the longitudinal pressure gradient to be constant across the flow, then it follows that u varies as the square root of the local depth:

$$u=\frac{\bar{u}\,h^{\frac{1}{2}}\bar{h}}{\overline{h^{\frac{3}{2}}}},\quad u_*=\frac{\bar{u}_*h^{\frac{1}{2}}\bar{h}}{\overline{h^{\frac{3}{2}}}}. \tag{9.1a,b}$$

The corresponding formula for the transverse turbulent diffusivity is

$$\kappa_{22}=\kappa_{\mathrm{T}}=\frac{\bar{\kappa}_{\mathrm{T}}h^{\frac{3}{2}}}{\overline{h^{\frac{3}{2}}}},$$

with

$$\bar{\kappa}_{\mathrm{T}}=0.15\bar{h}\bar{u}_*. \tag{9.2}$$

here $\bar{h}$ and $\bar{\kappa}_{\mathrm{T}}$ are averages without the usual depth weighting, and the numerical factor 0.15 is based upon the experiments of Sumer (1976). For later use we have introduced the notation κ_{T} to denote the turbulence contribution to κ_{22}.

One class of flows for which the eigenfunction equations (7.1*a–e*) are easy to solve, is when the geometry is self-similar at all transects:

$$h=\frac{\bar{h}(x)\,h_0(y)}{\bar{h}_0},\quad m_1=1. \tag{9.3}$$

Self-similarity is not quite as restrictive as assuming that the channel is of constant

width, because in flow-following coordinates the actual width enters via the metric coefficient

$$m_2 = \frac{B}{B_0}, \tag{9.4a}$$

with

$$y_L - y_R = 2B_0, \tag{9.4b}$$

$$B\bar{h}\bar{u} = \text{constant}. \tag{9.4c}$$

With the assumptions (9.1)–(9.3), the generalized eigenfunctions are the same as the conventional (straight-channel) cross-stream advection–diffusion modes

$$\phi_n^{(+)} = \phi_n^{(-)} = \phi_n^{(0)}(y), \tag{9.5}$$

and the x-dependence is relegated to the eigenvalue:

$$\frac{\mathrm{d}}{\mathrm{d}y}\left(h_0^{\frac{5}{2}}\frac{\mathrm{d}}{\mathrm{d}y}\phi_n^{(0)}\right) + \frac{\lambda_n h_0^{\frac{3}{2}}\bar{h}_0}{B_0^2}\phi_n^{(0)} = 0, \tag{9.6a}$$

with

$$h_0^{\frac{5}{2}}\frac{d\phi_n^{(0)}}{\mathrm{d}y} = 0 \quad (y = y_R, y_L), \tag{9.6b}$$

$$\frac{1}{y_L - y_R}\int_{y_R}^{y_L}\frac{h_0^3}{\bar{h}_0^3}\phi_n^{(0)2}\mathrm{d}y = 1, \tag{9.6c}$$

$$\frac{1}{y_L - y_R}\int_{y_R}^{y_L}\frac{h_0^3}{\bar{h}_0^3}\phi_n^{(0)}\phi_m^{(0)}\mathrm{d}y = 0 \quad (m \neq n), \tag{9.6d}$$

$$\mu_n^{(0)}(x) = 0.15\lambda_n\frac{\bar{u}_*}{\bar{u}}\frac{\bar{h}(x)}{B(x)^2}. \tag{9.6e}$$

It is the small values of the ratios $\bar{u}_*/\bar{u}$ and $\bar{h}/B$ that make the diffusion lengthscale $1/\mu_1$ so much greater than the channel breadth.

For this class of flows $\overline{\phi_n^{(+)}} = \overline{\phi_n^{(-)}} = \overline{\phi_n^{(0)}}$ is constant, and therefore the local dispersion coefficient (7.7) is strictly positive:

$$D_{\mathrm{loc}} = \bar{u}(x)^2\sum_{n=1}^{\infty}\int_{-\infty}^{x}\frac{(\overline{\phi_n^{(0)}})^2}{\bar{u}(x')}\exp\left(-\int_{x'}^{x}\mu_n(x'')\mathrm{d}x''\right)\mathrm{d}x'. \tag{9.7}$$

Downstream of a sudden change in flow conditions (velocity ratio $\bar{u}_*/\bar{u}$, depth- or widthscale), the multiplicative factor $\bar{u}(x)^2$ can be taken to be constant. Thus, the qualitative behaviour of D_{loc} depends upon the change in $1/\mu_n\bar{u}$, or equivalently upon the change in B^3. If the breadth increases then the memory integral increases downstream. Hence, after the change in breadth, D_{loc} increases towards its asymptote. Figure 2(*a*) corresponds to a breadth increase, and figure 2(*b*) to a combined depth and breadth increase. In the opposite circumstance of a reduction in breadth, the memory integral decreases downstream. Thus, after the change in breadth, D_{loc} decreases towards its asymptote (figure 3*a*, *b*). It is noteworthy that in the combined depth and breadth increase (figure 3*b*), there is a region of anomalously large longitudinal dispersion. Physically the strong velocity shear downstream of the change is acting upon the relatively large concentration variation c_1 that was generated upstream of the constriction.

A parabolic depth profile

$$h_0 = \tfrac{3}{2}\bar{h}_0\left[1 - \left(\frac{y}{B_0}\right)^2\right], \quad y_R = -B_0, \quad y_L = B_0, \tag{9.8}$$

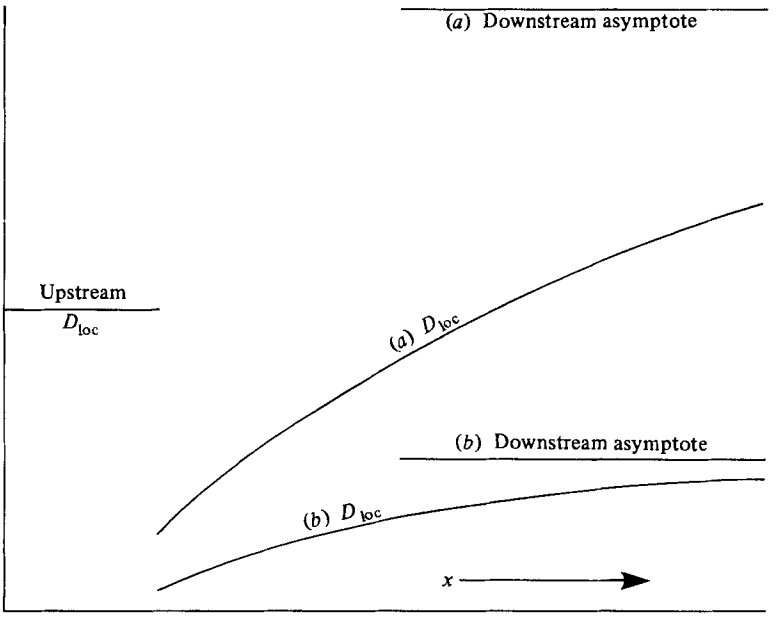

FIGURE 2. Longitudinal-dispersion coefficient when there is a sudden increase in channel breadth.

has the virtues of resembling many natural depth profiles and being analytically tractable. The normalized eigenfunctions are Gegenbauer polynomials:

$$\phi_n^{(0)} = \left[\frac{3}{(n+1)(n+3)}\right]^{\frac{1}{2}} C_n^{(2)}\left(\frac{y}{B_0}\right), \tag{9.9a}$$

with

$$\lambda_n = \tfrac{3}{2}n(n+4), \tag{9.9b}$$

$$\overline{\phi_n^{(0)}} = 0 \quad (n \text{ odd}), \tag{9.9c}$$

$$\overline{\phi_n^{(0)}} = \tfrac{1}{2}(n+2)\left[\frac{3}{(n+1)(n+3)}\right]^{\frac{3}{2}} \quad (n \text{ even}) \tag{9.9d}$$

(Gradshteyn & Ryzhik 1965, §§7.31, 8.93). The results shown in figures 2(*a*), 3(*a*) correspond to a factor-of-two breadth change with constant depth, while in figures 2(*b*), 3(*b*) the breadth and depth both change by the same factor two. In all cases the upstream conditions are taken to be the same. The rapid increase of λ_n with modenumber means that the value of D_{loc} is dominated by the lowest even mode $n = 2$.

10. Curvature effects

As well as pointing out the memory character of the longitudinal dispersion process, Fischer (1969) also demonstrated the importance of centrifugal effects as regards the transverse dispersion. The radial pressure gradient induces a secondary flow (outwards near the free surface, with a return current near the channel bed). Fischer (1969, equation (8)) shows that the contaminant flux associated with this transverse circulation is equivalent to increasing κ_{22} by an amount

$$30h^3\rho^2 u\frac{u}{u_*}, \tag{10.1}$$

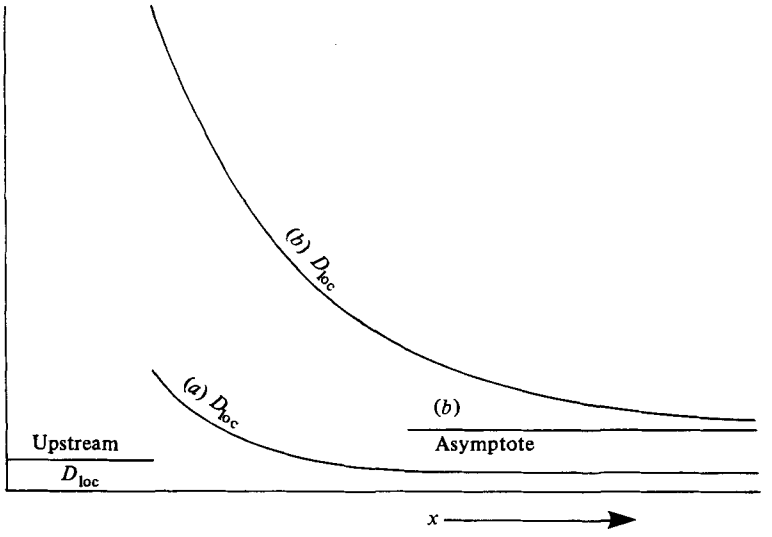

FIGURE 3. Longitudinal-dispersion coefficient when there is a sudden decrease in channel breadth.

where $\rho(x)$ is the channel curvature (the reciprocal of the radius of curvature). Strictly, Fischer's result involves both the Darcy–Weisbach factor f and the von Kármán constant k. The stated result (10.1) corresponds to the parameter values

$$f = 0.04, \quad k = 0.4. \tag{10.2}$$

To retain the mathematical simplicity of the self-similar case, we shall model the effects of curvature as increasing the transverse-dispersion coefficient κ_{22} from its turbulent value κ_T to

$$\kappa_{22} = \kappa_T(1 + F(x)). \tag{10.3}$$

Comparing the average of the increment (10.1) with the empirical formula (9.2) leads us to define this curvature factor (Fischer number)

$$F = 200(\bar{h}\rho)^2\left(\frac{\bar{u}}{\bar{u}_*}\right)^2. \tag{10.4}$$

Thus, if the velocity ratio $\bar{u}/u_*$ remains constant, then (9.6e) gains a new factor $1 + F(x)$ in the decay exponent

$$\mu_n(x) = 0.15\lambda_n(1 + F(x))\frac{\bar{u}}{\bar{u}_*}\frac{\bar{h}(x)}{B(x)^2}. \tag{10.5}$$

To isolate the dependence of D upon curvature, we take B, h to be constant, and ρ to vary sinusoidally:

$$F(x) = \hat{F}\sin^2 lx. \tag{10.6}$$

Evaluating the inner integral, we find that (7.7) now becomes

$$D_{loc} = \frac{\bar{u}^2B^2}{\bar{\kappa}_T}\sum_{n=1}^{\infty}(\overline{\phi_n^{(0)}})^2\int_0^{\infty}\exp\left(\tfrac{1}{2}\lambda_n\left\{[2+\hat{F}]\chi - \frac{\hat{F}}{\gamma}\sin\gamma\chi\cos(\gamma\chi - 2lx)\right\}\right)d\chi, \tag{10.7}$$

where

$$\gamma = \frac{lB^2\bar{u}}{\bar{\kappa}_T} \tag{10.8}$$

is the bend wavenumber relative to the diffusion lengthscale (cf. Fisher 1969,

equation (11)). The averaging with respect to x can be performed explicitly (Gradshteyn & Ryzhik 1965, §3.937.2):

$$D = \frac{\bar{u}^2 B^2}{\bar{\kappa}_T} \sum_{n=1}^{\infty} (\overline{\phi_n^{(0)}})^2 \int_0^{\infty} \exp(-\tfrac{1}{2}\lambda_n[2+\hat{F}]\chi) I_0\left(\tfrac{1}{2}\lambda_n\left(\frac{\hat{F}}{\gamma}\right)\left|\sin\gamma\chi\right|\right) d\chi, \tag{10.9}$$

where I_0 is the associated Bessel function of order zero.

In the limit of small γ (i.e. of long bends), we can replace $\sin\gamma\chi$ by $\gamma\chi$ in the argument of the associated Bessel function, and we can use equation (6.611.4) of Gradshteyn & Ryzhik (1965) to obtain

$$D = \frac{\bar{u}^2 B^2}{\bar{\kappa}_T}\left(\sum_{n=1}^{\infty} \frac{(\overline{\phi_n^{(0)}})^2}{\lambda_n}\right)\frac{1}{[1+\hat{F}]^{\frac{1}{2}}}. \tag{10.10a}$$

For channels of parabolic cross-section we can sum the series:

$$D = \frac{0.012\dfrac{\bar{u}^2 B^2}{\bar{h}\bar{u}_*}}{[1+\hat{F}]^{\frac{1}{2}}} \tag{10.10b}$$

for

$$\gamma \ll \lambda_2 = 18. \tag{10.10c}$$

In the opposite limit of short bends we can replace I_0 by unity to derive the asymptote

$$D = \frac{\bar{u}^2 B^2}{\bar{\kappa}_T}\left(\sum_{n=1}^{\infty} \frac{(\overline{\phi_n^{(0)}})^2}{\lambda_n}\right)\frac{1}{[1+\frac{1}{2}\hat{F}]}, \tag{10.11a}$$

$$= \frac{0.012(\bar{u}^2 B^2/\bar{h}\bar{u}_*}{[1+\frac{1}{2}\hat{F}]} \tag{10.11b}$$

for

$$\gamma \gg \lambda_2 = 18. \tag{10.11c}$$

For small $\hat{F}$ the two formulae agree. However, when the curvature effect is large the dispersion coefficient is significantly larger in the long-bend case (10.10). The reason for this is that where the curvature changes sign the mixing remains comparatively inefficient. The eventual reduction in D as $\hat{F}^{-\frac{1}{2}}$ is a consequence of the diminishing size of this region in which curvature remains insignificant. For the short-bend case (10.11) it is the averaged rate of mixing that matters (see (8.6*b*)). It is this averaging of $1+\hat{F}\sin^2 lx$ which gives rise to the $1+\frac{1}{2}\hat{F}$ factor in the denominator of (10.11*a*).

This difference in character between long- and short-bend results helps to explain why it has proved impossible to collapse field data for D onto a single empirical curve (Fukuoka & Sayre 1973). To date the best empirical formulae for the longitudinal-dispersion coefficient in natural streams would seem to be that of Fischer (1975), which can under- or overestimate D by as much as a factor of four. It is hoped that the present calculations might provide a theoretical basis for some new empirical formula for D.

11. Changes in depth profile

If the y-coordinate is genuinely flow-following, then from the model (9.1a) for the velocity distribution we infer that

$$m_2 = \frac{B\overline{h^{\frac{3}{2}}}h_0^{\frac{3}{2}}}{B_0\overline{h_0^{\frac{3}{2}}}h^{\frac{3}{2}}}, \tag{11.1}$$

where $h_0(y), B_0$ are the reference depth profile and breadthscale at a location where $m_2 = 1$. If in addition the diffusivity distribution is given by the model (9.2), and the channel is sufficiently straight that we can set $m_1 = 1$, then the field equation (7.1a) for the eigenmode $\phi_n^{(+)}(x, y)$ can be written

$$0.15\frac{\bar{u}_*}{\bar{u}}\left(\frac{B_0}{B}\right)^2\frac{\overline{h_0^{\frac{3}{2}}}}{(\overline{h^{\frac{3}{2}}})^2}\frac{\partial}{\partial y}\left(\frac{h^4}{h_0^{\frac{3}{2}}}\frac{\partial}{\partial y}\phi_n^{(+)}\right)+\mu_n\frac{h_0^{\frac{3}{2}}}{\overline{h_0^{\frac{3}{2}}}}\phi_n^{(+)} = \frac{h_0^{\frac{3}{2}}}{\overline{h_0^{\frac{3}{2}}}}\partial_x\phi_n^{(+)}. \tag{11.2}$$

The resemblance to the self-similar case leads us to pose the representations (cf. Smith 1982, §6)

$$\phi_n^{(+)} = \phi_n^{(0)}(y)+\sum_{m=1}^{\infty} a_{nm}^{(+)}(x)\,\phi_m^{(0)}(y), \tag{11.3a}$$

$$\phi_n^{(-)} = \phi_n^{(0)}(y)+\sum_{m=1}^{\infty} a_{nm}^{(-)}(x)\,\phi_m^{(0)}(y), \tag{11.3b}$$

$$\mu_n = \mu_n^{(0)}+\mu_n'. \tag{11.3c}$$

The $\phi_m^{(0)}$ component of (11.2) yields coupled ordinary differential equations for the coefficients $a_{nm}^{(+)}$:

$$\partial_x a_{nn}^{(+)} = -2\mu_n^{(0)}H_{nn}+\mu_n'-\sum_{m=1}^{\infty}(\mu_m^{(0)}+\mu_n^{(0)})\,H_{nm}a_{nm}^{(+)}+\mu_n' a_{nn}^{(+)}, \tag{11.4}$$

$$\partial_x a_{nm}^{(+)} = -(\mu_m^{(0)}+\mu_n^{(0)})\,H_{nm}+(\mu_n^{(0)}-\mu_m^{(0)})\,a_{nm}^{(+)}-\sum_{j=1}^{\infty}(\mu_j^{(0)}+\mu_m^{(0)})\,H_{mj}a_{nj}^{(+)}+\mu_n' a_{nm}^{(+)}. \tag{11.4b}$$

Here the H_{mj} terms are related to the departure from self-similarity of the depth profile:

$$H_{mj} = \frac{B_0}{2(\lambda_m+\lambda_j)}\int_{y_R}^{y_L}\left(\frac{\overline{h_0^{\frac{3}{2}}}}{\bar{h}(\overline{h^{\frac{3}{2}}})^2}\frac{h^4}{h_0^{\frac{3}{2}}}-\frac{h_0^{\frac{5}{2}}}{\bar{h}_0\overline{h_0^{\frac{3}{2}}}}\right)\partial_y\phi_m^{(0)}\,\partial_y\phi_j^{(0)}\,\mathrm{d}y. \tag{11.5}$$

The corresponding equations for $a_{nn}^{(-)}, a_{nm}^{(-)}$ have reversed x-derivatives but the same coefficients. The constraint (7.1e) upon the x-dependence of the upstream and downstream modes can be transformed into an equation for μ_n':

$$\begin{aligned}\mu_n'\left[1+\tfrac{1}{2}(a_{nn}^{(+)}+a_{nn}^{(-)})+\sum_{m=1}^{\infty}a_{nm}^{(+)}a_{nm}^{(-)}\right] &= 2\mu_n^{(0)}H_{nn}+\sum_{m=1}^{\infty}(\mu_m^{(0)}+\mu_m^{(0)})\,H_{nm}(a_{nm}^{(+)}+a_{nm}^{(-)})\\ &\quad-\sum_{m=1}^{\infty}a_{nm}^{(+)}a_{nm}^{(-)}(\mu_n^{(0)}-\mu_m^{(0)})\\ &\quad+\sum_{m=1}^{\infty}\sum_{j=1}^{\infty}(\mu_n^{(0)}+\mu_j^{(0)})\,H_{jn}a_{nm}^{(+)}a_{nj}^{(-)}.\end{aligned} \tag{11.6}$$

(We note that the equivalent equation (31) of Smith (1982) is in error, but has no effect upon the selection of optimal discharge sites.)

A limiting case in which (11.4a,b) become analytically tractable is when the departure from self-similarity is moderately small. In this case we can linearize (11.4a,b) by the neglect of all mixed terms $H_{mj}a_{nj}^{(+)}, \mu_n' a_{nm}^{(+)}$. Also, from (11.6) we have the linear approximation

$$\mu_n' = 2\mu_n^{(0)}H_{nn}. \tag{11.7}$$

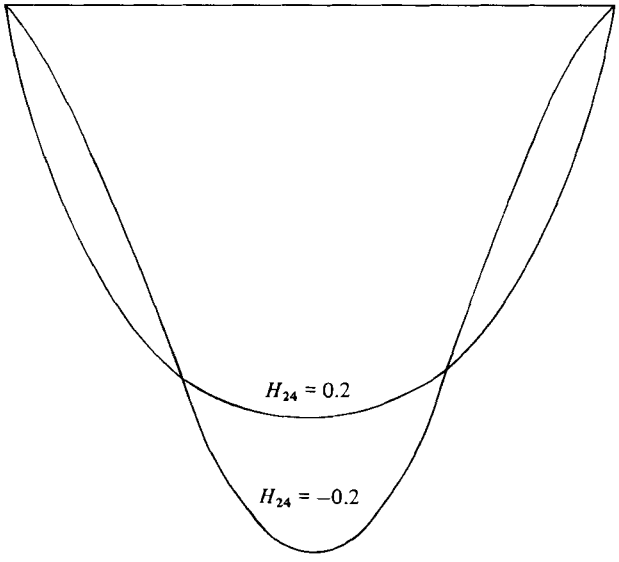

FIGURE 4. Depth profiles with the flatness parameter $H_{24} = \frac{1}{5}, -\frac{1}{5}$.

The resulting explicit solutions for the coefficients $a_{nm}^{(+)}, a_{nm}^{(-)}$ are

$$a_{nn}^{(+)} = a_{nn}^{(-)} = 0, \tag{11.8a}$$

$$a_{nm}^{(+)} = -a_{mn}^{(-)} = -\int_{-\infty}^{x} \exp\left(-\int_{x'}^{x} (\mu_m^{(0)} - \mu_n^{(0)})\,\mathrm{d}x''\right) H_{nm}(x')\,(\mu_m^{(0)} + \mu_n^{(0)})\,\mathrm{d}x' \quad (n < m) \tag{11.8b}$$

$$a_{nm}^{(-)} = -a_{mn}^{(+)} = -\int_{x}^{\infty} \exp\left(-\int_{x}^{x'} (\mu_m^{(0)} - \mu_n^{(0)})\,\mathrm{d}x''\right) H_{nm}(x')\,(\mu_m^{(0)} + \mu_n^{(0)})\,\mathrm{d}x' \quad (n < m). \tag{11.8c}$$

Substituting the representations (11.3a, b) into the general expression (7.7) and then neglecting quadratic terms $a_{nm}^{(+)} a_{nl}^{(-)}$, we have the linear approximation

$$\begin{aligned} D_{\mathrm{loc}} = \bar{u}(x)^2 \sum_{n=1}^{\infty} (\overline{\phi_n^{(0)}})^2 \int_{-\infty}^{x} \mathrm{d}x' \exp\left(-\int_{x'}^{x} \mu_n^{(0)}(x'')\,\mathrm{d}x''\right) \Big/ \bar{u}(x') \\ + \bar{u}^2 \sum_{n=1}^{\infty} \sum_{m=1}^{\infty} \overline{\phi_n^{(0)}}\, \phi_m^{(0)} \left\{ a_{nm}^{(+)} \int_{-\infty}^{x} \mathrm{d}x' \exp\left(-\int_{x'}^{x} \mu_n^{(0)}(x'')\,\mathrm{d}x''\right) \Big/ \bar{u}(x') \right. \\ \left. + \int_{-\infty}^{x} \mathrm{d}x' a_{mn}^{(-)}(x') \exp\left(-\int_{x'}^{x} \mu_m^{(0)}(x'')\,\mathrm{d}x''\right) \Big/ \bar{u}(x') \right\}. \end{aligned} \tag{11.9}$$

Since the $a_{nm}^{(+)}, a_{nm}^{(-)}$ coefficients can depend upon H_{nm} downstream of x (see (11.8c)), it is by no means obvious that D_{loc} is causal. Yet the definition (6.4) of D_{loc} in terms of the shape factor G is clearly causal. This superficial difficulty can be resolved if we use the explicit solutions (11.8b, c) for $a_{mn}^{(+)}, a_{mn}^{(-)}$. The downstream terms all cancel and we are left with the causal expression

$$\begin{aligned} D_{\mathrm{loc}} = \bar{u}(x)^2 \sum_{n=1}^{\infty} (\overline{\phi_n^{(0)}})^2 \int_{-\infty}^{x} \mathrm{d}x' \exp\left(-\int_{x'}^{x} \mu_n^{(0)}(x'')\,\mathrm{d}x'\right) \Big/ \bar{u}(x') \\ - \bar{u}(x)^2 \sum_{n=1}^{\infty} \sum_{m>n} \overline{\phi_n^{(0)}}\, \overline{\phi_m^{(0)}} \int_{-\infty}^{x} H_{nm}(x')\,(\mu_m^{(0)} + \mu_n^{(0)})\, I_{nm}(x, x')\,\mathrm{d}x', \end{aligned} \tag{11.10a}$$

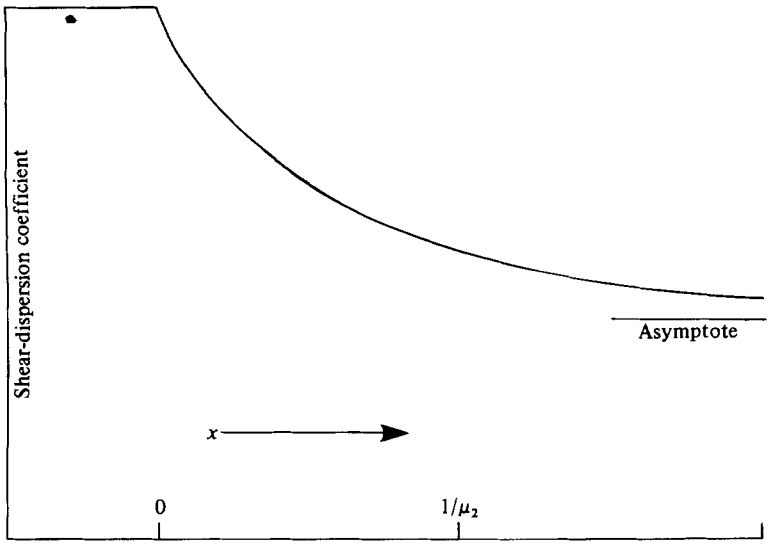

FIGURE 5. The change in dispersion coefficient when the flatness parameter jumps from $H_{24} = 0$ to $H_{24} = \frac{1}{2}$.

with

$$I_{nm} = \exp\left(-\int_{x'}^{x}\mu_m^{(0)}(x'')\,dx''\right)\int_{-\infty}^{x'} dx'' \exp\left(-\int_{x''}^{x'}\mu_n^{(0)}(\tilde{x})\,d\tilde{x}\right)\Big/\bar{u}(x'')$$
$$+\exp\left(-\int_{x'}^{x}\mu_n^{(0)}(x'')\,dx''\right)\int_{-\infty}^{x'} dx'' \exp\left(-\int_{x''}^{x'}\mu_m^{(0)}(\tilde{x})\,d\tilde{x}\right)\Big/\bar{u}(x''). \quad (11.10b)$$

For a symmetric reference depth profile the odd $\overline{\phi_n^{(0)}}$ coefficients are zero (see (9.9*c*)). Thus the leading correction to the self-similar result (9.7) for $D_{\rm loc}$ arises at H_{24}. From (11.5*b*) we can infer that H_{24} is positive or negative accordingly as the depth profile is flatter-bottomed or steeper than the reference profile. Figure 4 shows two profiles with $H_{24} = 0.2, -0.2$. Slight asymmetry does not effect H_{24}, as a consequence of the symmetry of the product $\partial_y\phi_2^{(0)}\partial_y\phi_4^{(0)}$.

In contrast with the spectacular change in $D_{\rm loc}$ associated with changes in breadth (see figures 2, 3), the response to a profile change is quite gradual. For example, if H_{24} suddenly increases from being zero at $x = 0$, then the resulting change to $D_{\rm loc}$ is given by the expression

$$H_{24}\overline{\phi_2^{(0)}}\,\overline{\phi_4^{(0)}}\,\bar{u}\left(\frac{1}{\mu_2^{(0)}}+\frac{1}{\mu_4^{(0)}}\right)[\exp(-\mu_2^{(0)}x)+\exp(-\mu_4^{(0)}x)-2]. \quad (11.11)$$

Thus the response is equally divided between the two lengthscales $1/\mu_2^{(0)}$ and $1/\mu_4^{(0)}$ of the lowest symmetric modes (see figure 5).

For sinusoidally changing depth profiles

$$H_{24} = \hat{H}_{24}\sin lx, \quad (11.12)$$

with all the other flow parameters constant, the oscillatory component of $D_{\rm loc}$ is given by

$$\frac{\bar{u}^2B^2}{\bar{\kappa}_{\rm T}}\hat{H}_{24}\left(\frac{1}{\lambda_2}+\frac{1}{\lambda_4}\right)\left[-\left\{\frac{\lambda_2^2}{\lambda_2^2+\gamma^2}+\frac{\lambda_4^2}{\lambda_4^2+\gamma^2}\right\}\sin lx+\left\{\frac{\gamma\lambda_2}{\lambda_2^2+\gamma^2}+\frac{\gamma\lambda_4}{\lambda_4^2+\gamma^2}\right\}\cos lx\right], \quad (11.13a)$$

with

$$\gamma = lB^2\bar{u}/\bar{\kappa}_{\rm T}. \quad (11.13b)$$

Thus, for long bends with $\gamma < \lambda_2$, the longitudinal dispersion coefficient is almost in phase with the depth profile (both vary as $\sin lx$). However, for short bends with $\gamma > \lambda_4$, the upstream memory of the dispersion coefficient is epitomized by the fact that D_{loc} is nearly out of phase with the changing depth profile (i.e. $\cos lx$ as opposed to $\sin lx$).

I wish to thank British Petroleum and the Royal Society for financial support.

REFERENCES

ELDER, J. W. 1959 The dispersion of marked fluid in turbulent shear flow. *J. Fluid Mech.* **5**, 544–560.

FISCHER, H. B. 1967 The mechanics of dispersion in natural streams. *J. Hydraul. Div. ASCE* **93**, 187–216.

FISCHER, H. B. 1969 The effect of bends on dispersion in streams. *Water Resources Res.* **5**, 496–506.

FISCHER, H. B. 1975 Simple method for predicting dispersion in streams. *J. Env. Engng Div. ASCE* **101**, 453–455.

FUKUOKA, S. & SAYRE, W. W. 1973 Longitudinal dispersion in sinuous channels. *J. Hydraul. Div. ASCE* **99**, 195–217.

GRADSHTEYN, I. S. & RYZHIK, I. M. 1965 *Table of Integrals, Series and Products.* Academic.

NAYFEH, A. H. 1973 *Perturbation Methods.* Interscience.

SMITH, R. 1977 Long-term dispersion of contaminants in small estuaries. *J. Fluid Mech.* **82**, 129–146.

SMITH, R. 1982 Where to put a steady discharge in a river. *J. Fluid Mech.* **115**, 1–11.

SUMER, S. M. 1976 Transverse dispersion in partially stratified tidal flow. *University of California, Berkeley, Hydraul. Engng Lab. Rep.* WHM-20.

TAYLOR, G. I. 1953 Dispersion of soluble matter in solvent flowing slowly through a tube. *Proc. R. Soc. Lond.* **A219**, 186–203.

YOTSUKURA, N. & COBB, E. D. 1972 Transverse diffusion of solutions in natural streams. *U.S. Geol. Survey Paper* no. 582-C.

YOTSUKURA, N. & SAYRE, W. W. 1976 Transverse mixing in natural channels. *Water Resources Res.* **12**, 695–704.